actuators

MDPI

Article

Implementation and Control of a Wheeled Bipedal Robot Using a Fuzzy Logic Approach

Chun-Fei Hsu [1,*], Bo-Rui Chen [2] and Zi-Ling Lin [1]

[1] Department of Electrical Engineering, Tamkang University, No. 151, Yingzhuan Rd., Tamsui Dist., New Taipei City 25137, Taiwan
[2] Department of Electrical and Computer Engineering, Institute of Electrical and Control Engineering, National Yang Ming Chiao Tung University, Hsinchu 30010, Taiwan
* Correspondence: fei@ee.tku.edu.tw

Abstract: This study designs and implements a wheeled bipedal robot (WBR) that combines the mobility of wheeled robots and the dexterity of legged robots. The designed WBR has extra knee joints to maintain body balance when encountering uneven terrain. Because of the robot's highly nonlinear, dynamic, unstable, and under-actuated nature, an intelligent motion and balance controller (IMBC) based on a fuzzy logic approach is proposed to maintain the balance of the WBR while it is standing and moving on the ground. It should be emphasized that the proposed IMBC system does not require prior knowledge of system dynamics and the controller parameters are tuned using the qualitative aspects of human knowledge. Furthermore, a 32-bit microcontroller that has memory, programmable I/O peripherals, and a processor core is used to implement the IMBC method. Finally, moving and rotating, height-changing, posture-keeping, and "one leg on slope" movement scenarios are tested to demonstrate the feasibility of the proposed IMBC system. The experimental results show that, by using the proposed IMBC system, the WBR can not only balance and move well both on flat ground and in complex terrain but also extend each leg independently to maintain body balance.

Keywords: fuzzy control; balance control; movement control; wheeled bipedal robot

Citation: Hsu, C.-F.; Chen, B.-R.; Lin, Z.-L. Implementation and Control of a Wheeled Bipedal Robot Using a Fuzzy Logic Approach. *Actuators* **2022**, *11*, 357. https://doi.org/10.3390/act11120357

Academic Editor: Matteo Cianchetti

Received: 29 October 2022
Accepted: 30 November 2022
Published: 2 December 2022

1. Introduction

Automation has become an integral part of all kinds of work, touting the benefits of not only reducing personnel costs but also maintaining the quality of the work done. In the past, industrial robots and human workers worked independently of each other in the workspace; however, robots and human workers will need to interact more directly in the future. Mechanisms for robot motion can be divided into two main domains: wheel-based approaches [1–3] and leg-based approaches [4–6]. Wheeled robots can change their position easily and quickly and their cost is lower; however, they cannot handle uneven terrain. Legged robots can travel almost anywhere but require heavy computational processing to actuate such complex movements. As they can achieve the advantages of both wheel- and leg-based designs, wheel-legged robots have attracted much attention [7–12]. The wheel-legged robot can move fast on flat ground and pass over uneven terrain, thereby improving the robot's adaptability in application scenarios. It also allows the robot's height to be changed to avoid collisions when it needs to pass under low obstacles.

Both academia and industry have conducted extensive research on self-balancing two-wheeled robots [13–15]. These have become an important member of the family of autonomous service robots, thanks to their good movement speed, load capacity, and terrain adaptability, and the concept has been successfully applied to transport robots [16] and hospitality robots [17,18]. Considering the diversity of locations, the wheeled bipedal robot (WBR) [19,20], which has two legs and two wheels (with the wheels installed on each foot), has more degrees of freedom than self-balancing two-wheeled robots [13–18] in the vertical direction. By achieving a higher movement speed and a larger movement

range, it is designed to be flexible even in the variable terrain of indoor environments. The most famous WBRs are "Handle" from Boston Dynamics and "Ascento" from ETH Zurich, which can move quickly on flat terrain, go down stairs, and jump through obstacles. However, because there are only two contact points between the robot and the ground, the ability to balance plays a key role in the practical application of WBRs.

Recently, there is increasing interest in studying the design, modeling, and control of WBRs. Traditional control schemes have been employed to solve the balance and height control issues [21–32]. A linear quadratic regulator (LQR) controller was designed to implement stabilization and driving control, and a proportional-integral-derivative (PID) controller was designed to synchronize the two leg motors in order to change the height of the robot [21]. However, these control gains needed to be pre-constructed using a tuning procedure. A cascade PID controller was proposed as the movement control system of a WBR [22]. Although it could achieve satisfactory balancing motion performance, it did not take into account how the WBR could pass over rough terrain. An easy-to-implement LQR-based control system was proposed [23–26]. However, the control performance degrades in the case of WBR operating point changes. An inverse dynamics controller was designed to consider the full dynamics of the WBR without neglecting any nonlinear dynamics terms [27]. However, these system uncertainties are unavoidable in a real WBR. A whole-body control frame was proposed for a WBR so that it could not only accelerate and decelerate along the forward direction and balance dynamically but also withstand disturbances more efficiently [28–32]. However, its control performance was highly dependent on the accuracy of the WBR's dynamic model.

The parameters of the model-based controller in recent studies [21–32] have had to be manually adjusted to ensure effective control when the physical parameters of the WBR change, such as robot height and payload weight. To overcome this shortcoming as well as solve the WBR balance problem, intelligent control schemes have been proposed [33–35]. A cascade PID controller was proposed for the path tracking of a WBR in which a reinforcement learning method automatically obtained optimal gains for the control law in a simulation [33]. Although the obtained controller gains could be directly applied in real-world scenarios without any re-training, the effect of robot height variation on the control response was not considered. A learning-based solution was proposed based on adaptive optimal control, where the controller parameters could be learned directly from the input-state data in the Gazebo robotic simulator [34]. However, it required heavy computational processing. An intelligent adaptive sliding-mode controller was proposed for the trajectory tracking and stability of a WBR, where a fuzzy-basis-function-network was used to approximate the system dynamics online [35]. However, the controller did not consider the effect of WBR height variation on the system response.

Fuzzy control (FC) using linguistic information can model the qualitative aspects of human knowledge and possesses several advantages, such as robustness, being model-free, and being a rule-based algorithm [36–38]. Most of the operations in an FC use error and change-of-error as the fuzzy input variables, where the rules table is constructed in a two-dimensional input space, which cause difficulties in implementation. It can be found that the rule tables have the skew–symmetry property, where the absolute magnitude of the control input is proportional to the distance from its main diagonal line in the normalized input space. To reduce the complexity of the implementation, a single-input fuzzy controller (SFC) was proposed based on the sliding-mode control scheme, where a new fuzzy input variable (called the signed distance) was derived [39–42]. Compared to FC system, the total number of fuzzy rules used in SFC system is greatly reduced, so the control rules can be easy to generate and adjust. However, due to the linguistic expression of the FC and SFC systems, it has not been easy to guarantee the stability and robustness of the closed-loop control systems.

This study proposes a WBR that consists of a body and two legs with wheels where each leg can be independently extended and retracted by driving a motor mounted on the hip of the body. It has the advantages of both leg and wheel movement, with good

maneuverability and a high load capacity. The height of the proposed WBR can be adjusted through the realization of a four-bar linkage. Since the four-bar linkage approximates the linear motion of the wheels perpendicular to the ground, the WBR can traverse simple terrain in the same manner as wheeled robots and adjust its posture to the shape of uneven ground.

To overcome the highly dynamic and under-actuated nature of the proposed WBR's behavior, this study proposes an intelligent motion and balance control (IMBC) system that comprises fuzzy movement balancing control (FMBC), fuzzy yaw steering control (FYSC), and fuzzy roll balancing control (FRBC). The FMBC, based on a dual-loop control structure, is designed to cope with the under-actuated nature problem of the WBR and allow the WBR to move at the desired velocity command while maintaining balance. The FYSC is a compensated speed control signal for the WBR that can rotate about its vertical axis, and the FRBC extends each leg independently to change the robot's height and altitude when driving over challenging terrain. Since the proposed IMBC method was designed based on the SFC method, it does not require complex analysis or heavy computational processing. A low-cost 32-bit STM32F446RE microcontroller is used to implement the control method for the WBR. Finally, four experimental scenarios are tested to explore the stability performance of the proposed IMBC system. The experimental results show that the proposed IMBC system is feasible and effective for robot motion on both flat and complex terrain.

The contribution of this study can be summarized as follows: (1) The mechanical structure of the WBR, which has two legs and two wheels (with the wheels installed on each foot), is designed and implemented. (2) An experimental setup is presented for the WBR using a low-cost 32-bit STM32F446RE microcontroller. (3) The IMBC system is shown to be able to maintain the balance of the WBR while standing and moving on the ground. (4) The IMBC system is shown to be able to independently control two leg motors to change the robot's height and attitude and allow the WBR to move over challenging terrain.

The remainder of this study is outlined as follows. In Section 2, the design and dynamic model of the WBR is presented. In Section 3, the structure of the IMBC system is presented. Experimental tests are presented in Section 4, and conclusions are given in Section 5.

2. System Structure and Modeling of the WBR

2.1. Mechanical Design

Figure 1 shows the mechanical structure of the WBR: Figure 1a shows the leg components and Figure 1b shows the kinematic models. The developed WBR, which consists of a body and two legs with wheels, is a promising way to improve the performance of bipedal robots in terms of flexibility, movement speed, and energy efficiency. By adding wheels to the ends of the legs, each leg can be independently extended and retracted by driving a leg motor mounted on the hip of the body. The torsion springs installed in the inner joints (see Figure 1a) are used to counteract the weight of the WBR itself, which can reduce the control effort of the leg motors when driving or standing to improve the overall efficiency of the robot. The total height of the WBR can be adjusted between 26 cm and 33 cm through the realization of a four-bar linkage.

In order to illustrate the relationship between the leg length of the WBR and the angle of the leg motor, part of the right leg is considered as shown in Figure 1b. The length between the pin joint and the inner joint, L_{kR}, can be found according to the Cosine law as follows:

$$L_{kR} = \sqrt{L_1^2 + L_2^2 - 2L_1L_2\cos\theta_{kR}} \quad (1)$$

where L_1 is the length between the pin joint and the knee joint, L_2 is the length between the pin joint and the leg joint, and θ_{kR} is the leg motor angle of the right leg. The torsion spring angle θ_{tR} and the length L_R of the right leg of the WBR can be found as follows:

$$\theta_{tR} = \pi - \cos^{-1}\left(\frac{L_1^2 + L_{kR}^2 - L_2^2}{2L_1L_{kR}}\right) - \cos^{-1}\left(\frac{L_3^2 + L_{kR}^2 - L_1^2}{2L_3L_{kR}}\right) \quad (2)$$

$$L_R = \sqrt{L_1^2 + L_4^2 - 2L_1L_4\cos(\theta_{tR})} \quad (3)$$

where L_3 is the length between the knee joint and the inner joint and L_4 is the length between the inner joint and the wheel motor. The height of the right side of the WBR is given as:

$$h_R = L_R + R \quad (4)$$

where R is the wheel radius. Similarly, the height of the left side of the WBR, h_L, can be obtained using the leg motor angle of the left leg θ_{kL} as follows:

$$h_L = \sqrt{L_1^2 + L_4^2 - 2L_1L_4\cos(\theta_{tL})} + R \quad (5)$$

in which

$$\theta_{tL} = \pi - \cos^{-1}\left(\frac{L_1^2 + L_{kL}^2 - L_2^2}{2L_1L_{kL}}\right) - \cos^{-1}\left(\frac{L_3^2 + L_{kL}^2 - L_1^2}{2L_3L_{kL}}\right) \quad (6)$$

$$L_{kL} = \sqrt{L_1^2 + L_2^2 - 2L_1L_2\cos\theta_{kL}} \quad (7)$$

where θ_{tL} is the torsion spring angle and L_{kL} is the length between the pin joint and the inner joint of the left leg of the WBR, respectively. Thus, the joint angles are adjusted to produce a change in the lengths of both sides of the robot (h_R and h_L) when the two leg motors are driven (θ_{kR} and θ_{kL}).

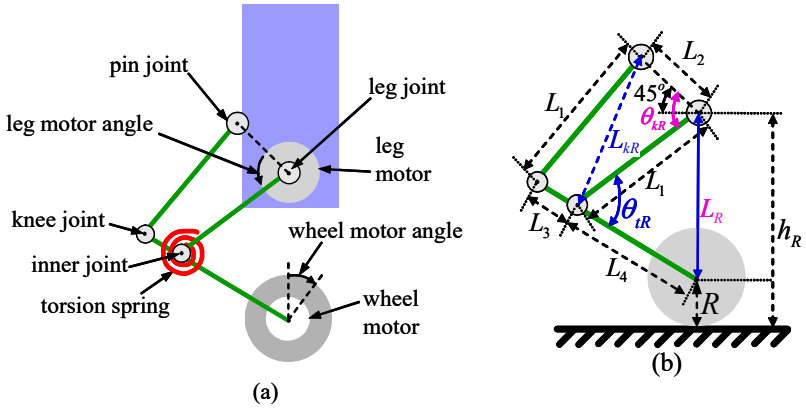

Figure 1. Mechanical structure. (**a**) Leg components. (**b**) Kinematic model of the right leg.

2.2. Hardware and Software

Figure 2 shows the photographs of the WBR: Figure 2a shows the WBR platform and Figure 2b shows the hardware connection diagram. The hardware connection diagram is composed of a STM32F446RE microcontroller, a MPU 6050, two wheel motors with optical encoders, and two leg motors. The MPU 6050, consisting of a 3-axis accelerometer and a 3-axis gyroscope, is located at the center of the robot body, the STM32F446RE microcontroller is placed on the upper body, and the motor drives are located on the lower body. The leg motor is a Dynamixel motor (MX-64) made by ROBOTIS, which can provide enough power for a leg to adjust the height of the robot. The wheel motor is a geared DC motor (GM25-370) made by ChiHai MOTOR, which can provide smooth stabilization and counteract disturbances to the tilt angle of the system. An encoder is installed behind the wheel motor to provide information on the robot's translational velocity and position. The MPU 6050 is used to measure the roll and pitch angles of the robot tilt. The STM32F446RE microcontroller, which is coded by Keil C, is used as a platform

for the implementation of control algorithms; it has a Cortex-M4 core, a processor clock frequency of up to 180 MHz, and a rich set of IO ports for connecting to various sensors and motors. The microcontroller, leg motors, wheel motors, and remaining electronic devices are powered by a 3-cell LiPo Battery.

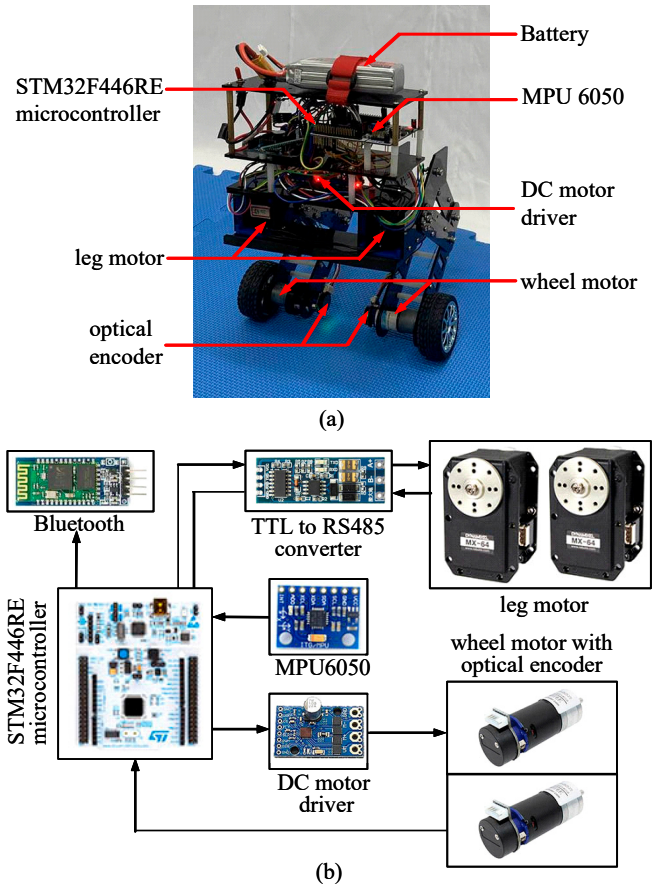

Figure 2. Photographs of the WBR. (**a**) WBR platform. (**b**) Hardware connection diagram.

2.3. Modeling

In order to manipulate the WBR, it is necessary to build a mathematical model that allows the robot and the designed controller to successfully achieve the desired control goals. Figure 3 shows the coordinate systems of the WBR and Appendix A lists all the symbols used and their definitions. The robot's position can be measured as $\theta_w = \frac{1}{2}(\theta_R + \theta_L)$ and the robot's body yaw angle ψ can be given as:

$$\psi = \frac{R}{2W}(\theta_R - \theta_L) \tag{8}$$

where θ_R is the rotary angle of the right wheel motor and θ_L is the rotary angle of the left wheel motor. The dynamic model of the WBR for the pitch axis can be described as [43]:

$$\mathbf{E}\begin{bmatrix}\ddot{\theta}_w \\ \ddot{\theta}\end{bmatrix} + \mathbf{F}\begin{bmatrix}\dot{\theta}_w \\ \dot{\theta}\end{bmatrix} + \mathbf{G}\begin{bmatrix}\theta_w \\ \theta\end{bmatrix} = \mathbf{H}\begin{bmatrix}v_L \\ v_R\end{bmatrix} + \mathbf{D} \tag{9}$$

where **E** is the inertia matrix, **F** is the matrix of centripetal and Coriolis forces, **G** is the gravity matrix, **H** is the gain matrix, **D** is the lump of uncertainties matrices (including the external disturbances and parameter uncertainties), and v_L and v_R are the input voltages of

the left and right wheel motors, respectively. These matrices can be found by considering the limits $\theta \to 0$, $\sin\theta \to \theta$ and $\cos\theta \to 1$ as:

$$\mathbf{E} = \begin{bmatrix} (2m+M)R^2 + 2J_w + 2J_m & MLR - 2J_m \\ MLR - 2J_m & ML^2 + J_\psi + 2J_m \end{bmatrix} \tag{10}$$

$$\mathbf{F} = 2\begin{bmatrix} \frac{K_t K_b}{R_m} & -\frac{K_t K_b}{R_m} \\ -\frac{K_t K_b}{R_m} & \frac{K_t K_b}{R_m} \end{bmatrix} \tag{11}$$

$$\mathbf{G} = \begin{bmatrix} 0 & 0 \\ 0 & -MgL \end{bmatrix} \tag{12}$$

$$\mathbf{H} = \begin{bmatrix} \frac{K_t}{R_m} & \frac{K_t}{R_m} \\ -\frac{K_t}{R_m} & -\frac{K_t}{R_m} \end{bmatrix} \tag{13}$$

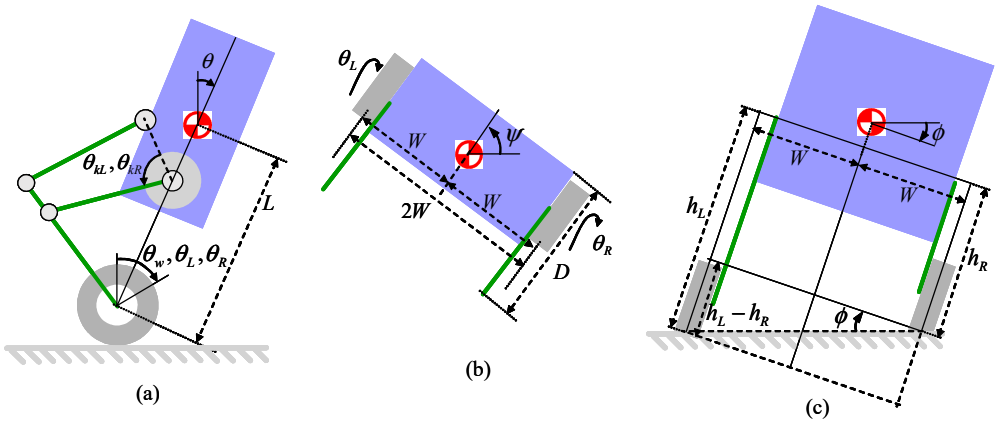

Figure 3. Generalized coordinates of the system. (**a**) Side view. (**b**) Top view. (**c**) Front view.

Equation (9) can be divided into two subsystems: one is the velocity control subsystem and the other is the balancing control subsystem. The velocity control subsystem is used to allow the WBR to move at the desired velocity command, and the balancing control subsystem is used to maintain the WBR's balance. Meanwhile, the dynamic model of the WBR for the yaw axis can be expressed as [43]:

$$\ddot{\psi} = -\frac{J}{I} + \begin{bmatrix} -\frac{K}{I} & \frac{K}{I} \end{bmatrix} \begin{bmatrix} v_L \\ v_R \end{bmatrix} \tag{14}$$

where $I = 2mW^2 + J_\phi + \frac{2W^2}{R^2}(J_w + J_m)$, $J = \frac{2W^2}{R^2}\frac{K_t K_b}{R_m}$, and $K = \frac{W}{R}\frac{K_t}{R_m}$. The robot body roll angle can be given as:

$$\phi = \tan^{-1}\left(\frac{h_L - h_R}{2W}\right) \tag{15}$$

When the robot's two legs are on the ground. From (9), (14) and (15), it shows the nonlinear and under-actuated nature of the WBR system. Since these robot parameters and the uncertainties matrix are unknown or perturbed in real WBR applications, a model-free control scheme should be designed that not only accelerates and decelerates along the forward direction and balances dynamically but is also robust to uncertainties.

3. Controller Design for the WBR

A dual-loop control structure was proposed to cope with the under-actuated nature problem of a self-balancing two-wheeled robot moving and turning while maintaining the robot's balance [43]. Extending the design ideas, this study proposes an IMBC system for the WBR, as shown in Figure 4. It comprises three controllers: FMBC, FYSC, and FRBC. It

is similar to [43], where the FMBC designed using a dual-loop control structure allows the WBR to move at the desired velocity command while maintaining balance and the FYSC can control the WBR to rotate about its vertical axis. Unlike [43], the FRBC is a novel design that independently controls two leg motors to change the robot's height and altitude and allows the WBR to travel over challenging terrain.

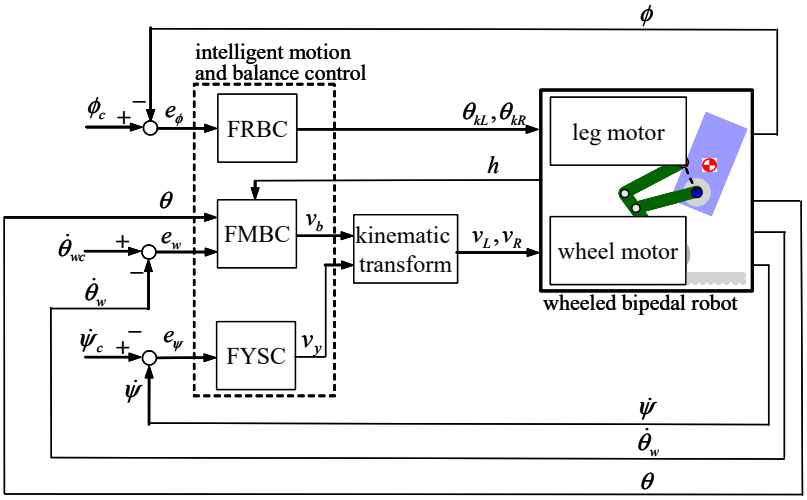

Figure 4. The block diagram of the IMBC system for the WBR.

3.1. FMBC Design

The FMBC should control the WBR to move at the desired velocity command and remain balanced even in the height variation of the WBR. A dual-loop control scheme is utilized, where the outer-loop controller (for the velocity control subsystem) is used to calculate the desired robot pitch angle for tracking velocity commands and the inner-loop controller (for the balancing control subsystem) is applied to keep the body balanced with the desired robot pitch angle. Thus, the advantage of the FMBC scheme lies in its simplicity and robust performance, compared to some other existing schemes [23–32]. According to the velocity command $\dot{\theta}_{wc}$ given by the users, an outer-loop sliding index is designed as [43]:

$$s_w = e_w + \lambda_1 \int_0^t e_w d\tau \tag{16}$$

where $e_w = \dot{\theta}_{wc} - \dot{\theta}_w$ is the translational velocity error and λ_1 is a positive constant. In order to converge the translational velocity error of the robot to zero quickly and have an excellent system response such as a faster rising time and smaller overshoot, each fuzzy rule of the outer-loop controller is given as follows:

$$\text{IF } s_w \text{ is } F_{sw}^i, \text{ THEN } \theta_c \text{ is } F_{\theta c}^i, \text{ for } i = 1, 2, \ldots, 7 \tag{17}$$

where F_{sw}^i are the labels of the fuzzy sets, $F_{\theta c}^i$ are the singleton control actions, and θ_c is the desired robot pitch angle. The fuzzy rules base of the outer-loop controller is given in Table 1, where the fuzzy labels are negative big (NB), negative medium (NM), negative small (NS), zero (ZO), positive small (PS), positive medium (PM), and positive big (PB), as shown in Figure 5a, where the membership functions of the fuzzy sets are given in a triangular form. The fuzzy rules in Table 1 are constructed using the idea that the outer-loop sliding index s_w can quickly reach zero via a time-consuming trial-and-error tuning procedure. The adopted outer-loop sliding index reduces the number of fuzzy rules, thus reducing the complexity of adjustment. It shows that the translational velocity error e_w will converge to zero when the outer-loop sliding index converges to zero. The outer-loop controller allows the WBR to move at the desired velocity command; thus, the velocity control subsystem can be asymptotically stable under the action of the outer-loop controller.

Table 1. The fuzzy rules for the FMBC.

s_w	NB	NM	NS	ZO	PS	PM	PB
$F^i_{\theta c}$	−15.0	−8.5	−5.4	0.0	5.4	8.5	15.0

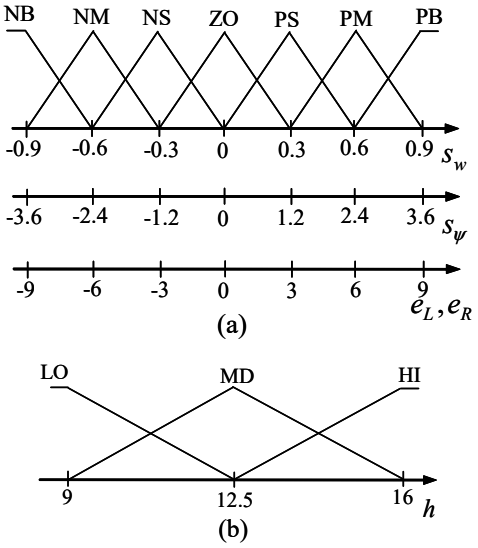

Figure 5. Membership functions. (**a**) FMBC and FRBC; (**b**) FYSC.

To cope with the system uncertainties caused by the changes in robot height, each fuzzy rule of the inner-loop controller is given as follows:

$$\text{IF } h \text{ is } F^j_h, \text{ THEN } v_b \text{ is } \mathbf{k}^T_j \mathbf{e}_\theta, \text{ for } j = 1, 2, \ldots, 3 \tag{18}$$

where the robot height can be measured as $h = \frac{1}{2}(h_R + h_L)$, F^j_h are the labels of the fuzzy sets, $e_\theta = \theta - \theta_c$ is the error of the body pitch angle, $\mathbf{e}_\theta = [e_\theta, \dot{e}_\theta]^T$ is the error vector, and $\mathbf{k}_j$ is the control gains vector of the inner-loop controller. The fuzzy labels used in this study are low (LO), medium (MD), and high (HI), as shown in Figure 5b, where the membership functions of the fuzzy sets are given in a triangular form. It is known that the outer-loop controller obtains the virtual angle command by defining the outer-loop sliding index and the inner-loop controller tracks the virtual angle command by defining the robot angle error. Thus, the balancing control subsystem can be asymptotically stable under the action of the inner-loop controller.

3.2. FYSC Design

FYSC is designed to control the WBR so that it can rotate along its vertical axis. The speed control signals applied to the right or left driving wheels are obtained as follows:

$$v_L = v_b + v_y \tag{19}$$

$$v_R = v_b - v_y \tag{20}$$

where v_b is the FMBC output and v_y is the FYSC output. According to the velocity command $\dot{\psi}_c$ given by the users, a yawing sliding index is designed as [43]:

$$s_\psi = e_\psi + \lambda_2 \int_0^t e_\psi d\tau \tag{21}$$

where the yaw speed error $e_\psi = \dot{\psi}_c - \dot{\psi}$ and λ_2 are positive constants. Each fuzzy rule of the FYSC is given as follows:

$$\text{IF } s_\psi \text{ is } F^i_{s\psi}, \text{ THEN } v_y \text{ is } F^i_{vy}, \text{ for } i = 1, 2, \ldots, 7 \tag{22}$$

where $F^j_{s\psi}$ are the labels of the fuzzy sets as shown in Figure 5a and F^i_{vy} are the singleton control actions. The fuzzy rules base of the FYSC is shown in Table 2, where it is constructed using the idea that the yawing sliding index s_ψ can quickly reach zero via a time-consuming trial-and-error tuning procedure. The adopted yaw sliding index reduces the number of fuzzy rules, thus reducing the complexity of adjustment. It shows that the yaw speed error e_ψ will converge to zero when the yaw sliding index converges to zero. The FYSC allows the WBR to rotate along its vertical axis at the desired velocity command. Thus, it can be asymptotically stable under the action of the FYSC.

Table 2. The fuzzy rules for the FYSC.

s_ψ	NB	NM	NS	ZO	PS	PM	PB
F^i_{vy}	−0.8	−0.3	−0.1	0.0	0.1	0.3	0.8

3.3. FRBC Design

When the ground is rough or the robot's legs are not of equal length, the FRBC is designed to control the WBR and maintain its horizontal posture and height by adjusting the length of its legs. Due to the hardware limitation, the WBR's leg length cannot be extended or shortened indefinitely. In the proposed WBR, the length of its legs can be adjusted between $h_{\max} = 161.1$ mm and $h_{\min} = 93.7$ mm through the realization of a four-bar linkage. When the leg length of the WBR is within the limitation, the FRBC is designed for posture control, and when the leg length of the WBR is on the limitation, the FRBC is designed for height control. First, considering the robot height is between $h_{\max}$ and $h_{\min}$, the FRBC is designed to control the WBR to maintain its horizontal posture. In the posture controller design, a rolling sliding index is designed as:

$$s_\phi = \dot{\phi} + \lambda_3 \phi \tag{23}$$

where λ_3 is a positive constant. Each fuzzy rule of the posture controller is given as follows:

$$\text{IF } s_\phi \text{ is } F^i_{s\phi}, \text{ THEN } \Delta\theta_{kL} \text{ is } F^i_{\phi L} \text{ and } \Delta\theta_{kR} \text{ is } F^i_{\phi R}, \text{ for } i = 1, 2, \ldots, 7 \tag{24}$$

where $F^i_{s\phi}$ are the labels of the fuzzy sets as shown in Figure 5a and F^i_L and F^i_R are the singleton control actions. The fuzzy rules base of the posture controller is shown in Table 3a, where it is constructed using the idea that the rolling sliding index s_ϕ can quickly reach zero via a time-consuming trial-and-error tuning procedure. The adopted rolling sliding index reduces the number of fuzzy rules, thus reducing the complexity of adjustment. It shows that the roll angle of the robot body ϕ will converge to zero when the rolling sliding index converges to zero. Thus, the FRBC allows the WBR to control two leg motors independently so as to maintain its horizontal posture.

Secondly, given that the height of either leg of the robot is at the limitations $h_{\max}$ or $h_{\min}$, the FRBC is designed to adjust the length of its legs to maintain its height. In order to ensure that the WBR can be kept at the setting height h_{set}, each fuzzy rule of the height controller can be designed as follows:

$$\text{IF } e_L \text{ is } F^i_{eL}, \text{ THEN } \Delta\theta_{kL} \text{ is } F^i_{hL} \tag{25}$$

$$\text{IF } e_R \text{ is } F^i_{eR}, \text{ THEN } \Delta\theta_{kR} \text{ is } F^i_{hR} \tag{26}$$

where $e_L = h_L - h_{set}$ and $e_R = h_R - h_{set}$ are the height errors, F^i_{eL} and F^i_{eR} are the labels of the fuzzy sets as shown in Figure 5a, and F^i_{hL} and F^i_{hR} are the singleton control actions. The fuzzy rules base is shown in Table 3b, where it is constructed using the idea that the height errors (e_L and e_R) can quickly reach zero by a time-consuming trial-and-error tuning procedure. This allows the WBR to control two leg motors independently in order to change the height of the robot while it is asymptotically stable under the action of FRBC. Thus, the motor angle of the left leg and the right leg are updated as follows:

$$\theta_{kL}(N+1) = \theta_{kL}(N) + \Delta\theta_{kL} \tag{27}$$

$$\theta_{kR}(N+1) = \theta_{kR}(N) + \Delta\theta_{kR} \tag{28}$$

where N denotes the number of iterations.

Table 3. The fuzzy rules for the FRBC.

(a) posture control							
s_ϕ	**NB**	**NM**	**NS**	**ZO**	**PS**	**PM**	**PB**
$\Delta\theta_{kL}$	−2.0	−1.5	−0.7	0.0	0.7	1.5	2.0
$\Delta\theta_{kR}$	2.0	1.5	0.7	0.0	−0.7	−1.5	−2.0
(b) height control							
e_L, e_R	**NB**	**NM**	**NS**	**ZO**	**PS**	**PM**	**PB**
$\Delta\theta_{kL}, \Delta\theta_{kR}$	−10	−7.5	−3.0	0.0	3.0	7.5	10

4. Experimental Results

The controller parameters of the IMBC system were selected as $\lambda_1 = 0.01$, $\lambda_2 = 0.125$, $\lambda_3 = 0.5$, $\mathbf{k}_1 = [130, 10]^T$, $\mathbf{k}_2 = [125, 10]^T$, and $\mathbf{k}_3 = [120, 10]^T$, considering the stability requirements and possible operating conditions. Generally, these control parameters require some trial-and-error tuning procedures to determine. To show the effectiveness of the IMBC system, a comparison between the cascade PID control [22] and the proposed IMBC system is presented. Four experimental scenarios (namely moving and rotating, height-changing, posture-keeping, and one leg on slope movement) were tested to explore the stability performance of the controllers. Figure 6 shows four photographs of the experiments, and the experimental results are discussed below.

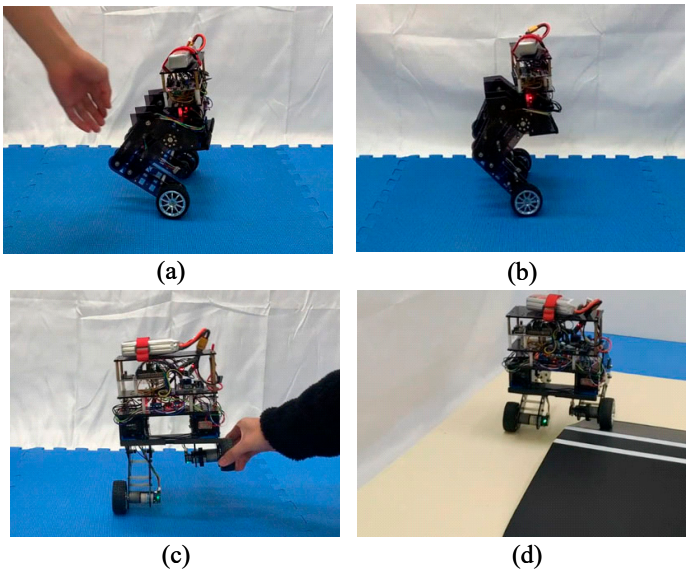

Figure 6. Photographs of the experiments: (**a**) moving and rotating; (**b**) height-changing; (**c**) posture-keeping; (**d**) one leg on slope movement.

4.1. Moving and Rotating Scenario

In this scenario, the WBR started by balancing in its initial posture at the setting height and staying at the setting height. The tests were then carried out, including self-balancing, station-keeping, anti-interference, moving, and rotating tests. The experiment was performed by executing three actions to demonstrate the flexibility of the WBR. Two external forces were pushed on both sides of its body by human hands at approximately the 3rd and 6th second. The WBR was then ordered to go forward for 3 s at the 12th second and turn right in place for 3 s at the 17th second. The experimental results of the moving and rotating scenario are shown in Figure 7a,b for the cascade PID control [22] and the IMBC system, respectively. These figures show that both the cascade PID control and the IMBC system are sufficiently robust against external disturbances and can perfectly perform tasks such as moving and rotating in place while maintaining good balance.

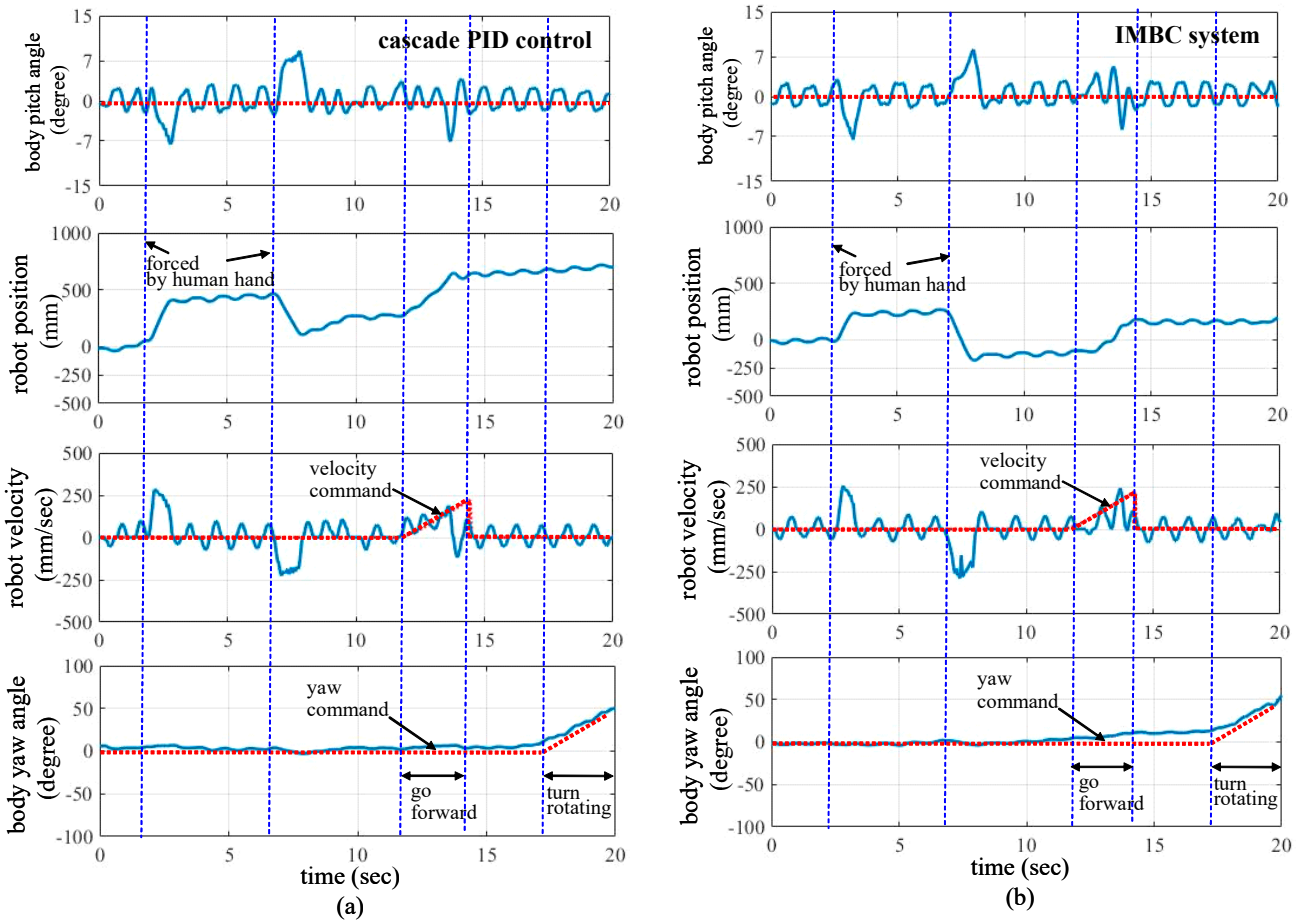

Figure 7. Results of moving and rotating. (**a**) Cascade PID control; (**b**) the IMBC system.

4.2. Height-Changing Scenario

In this scenario, the WBR started balancing in its initial posture at the minimum height. The experiment was performed by increasing the height of the robot to the maximum height starting at approximately the 2nd second and then changing the height of the robot to the minimum height at approximately the 4th second. The experimental results of the height-changing scenario are shown in Figure 8a,b for the cascade PID control [22] and the IMBC system, respectively. It can be seen that when the robot height command is changed, the length of both legs increases or decreases at the same time. Comparing Figure 8a,b shows that the WBR was able to stay in place without generating significant motion when using the proposed IMBC system. However, when using the cascade PID control, the robot could not stay in its original position, owing to the change in height of its center of gravity.

This result demonstrates that the proposed IMBC system can effectively overcome the effects of system uncertainties caused by robot height variations.

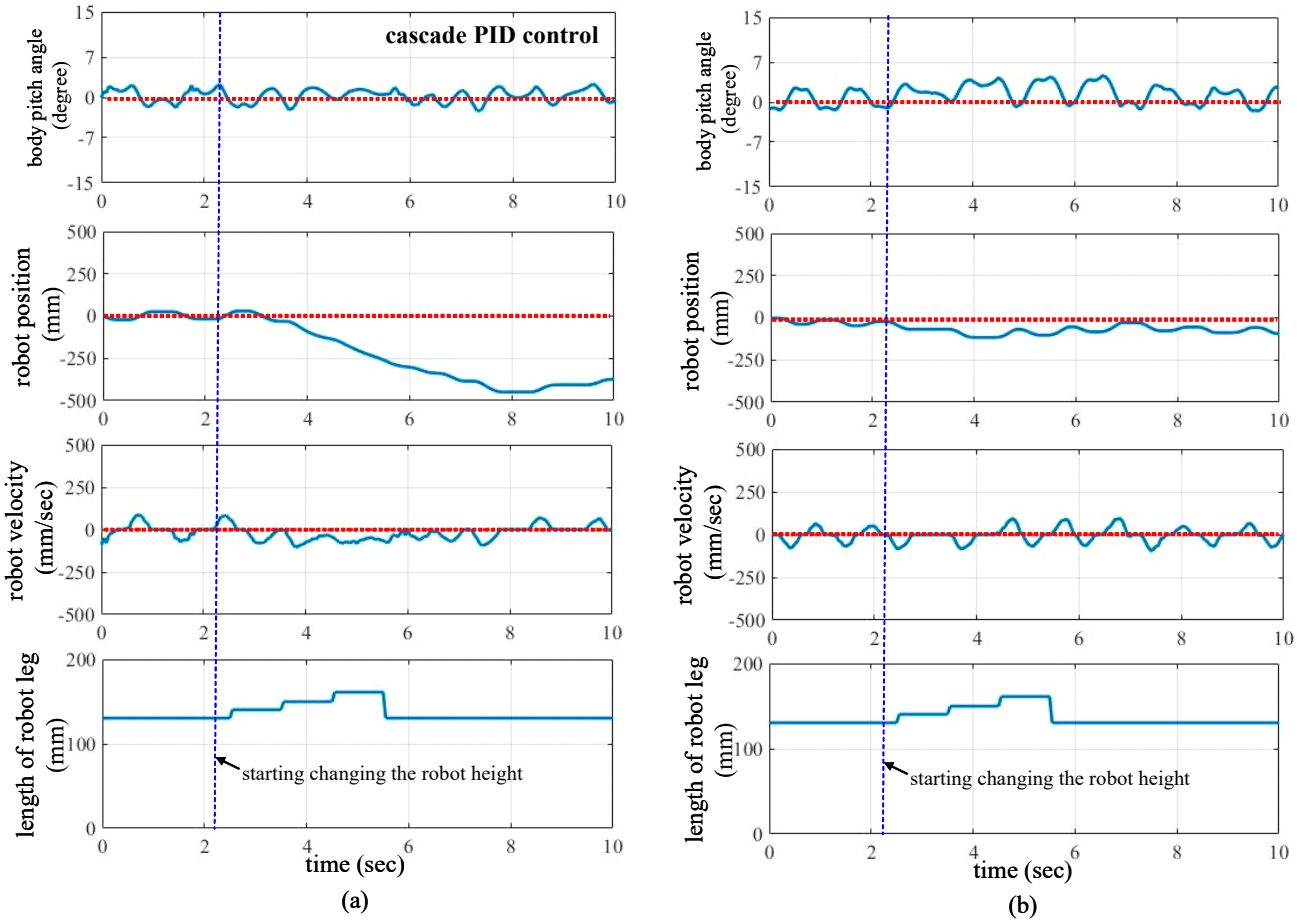

Figure 8. Results of height changing. (**a**) Cascade PID control; (**b**) the IMBC system.

4.3. Posture-Keeping Scenario

The robustness of the IMBC system was tested when one wheel was slightly off the ground. The purpose of the experiment was to test whether the leg strategy controller could maintain the robot's height when it was disturbed by human hands. The experiment was performed by lifting the right foot of the WBR by hand at approximately the 2nd second and putting it down at approximately the 6th second, and then lifting the left foot of the WBR by hand at approximately the 12th second and putting it down at approximately the 16th second. The experimental results of the posture-keeping scenario are shown in Figure 9a,b for the cascade PID control [22] and the IMBC system, respectively. They show that the proposed IMBC system can maintain the horizontal posture of the WBR during the leg lifting process, and when the single leg on one side of the leg lift reaches its limit, the other side can be extended or retracted to compensate for the error of the horizontal angle. Because the cascade PID controller cannot independently control two leg motors to change the robot's attitude, the horizontal posture of the WBR cannot be maintained during the leg lifting process.

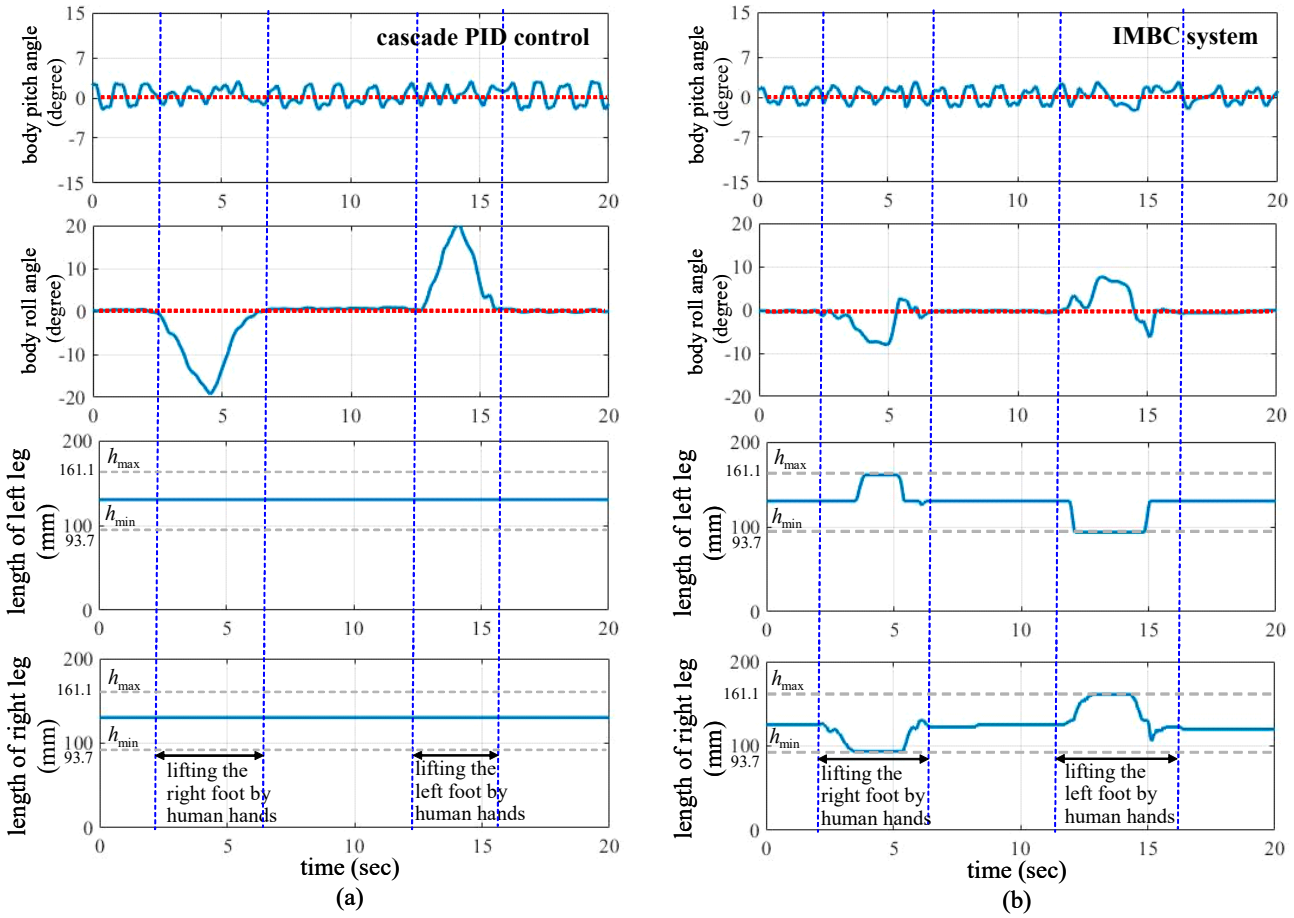

Figure 9. Results of body balancing. (**a**) Cascade PID control; (**b**) the IMBC system.

4.4. One Leg on Slope Movement Scenario

The WBR moved on a small slope of approximately 12° on one side and 8° on the other side, with the left leg on the small slope and the right leg on the flat ground. The purpose of the experiment was to test whether the leg strategy controller could keep the robot horizontal when it was disturbed by terrain. The experiment had the robot move forward at approximately the 5th second with the left foot on the ramp but the right foot on the ground and then move backward to its original position at approximately the 7th second. The experimental results of the posture-keeping scenario are shown in Figure 10a,b for the cascade PID control [22] and the IMBC system, respectively. These results show that the proposed IMBC system can adjust the height of the left and right legs in time to avoid the robot falling over as a result of a change in height of the left and right leg positions. However, the cascaded PID controller cannot adjust the height of the left and right legs independently, so when the WBR is disturbed by terrain changes, its balance can easily fail.

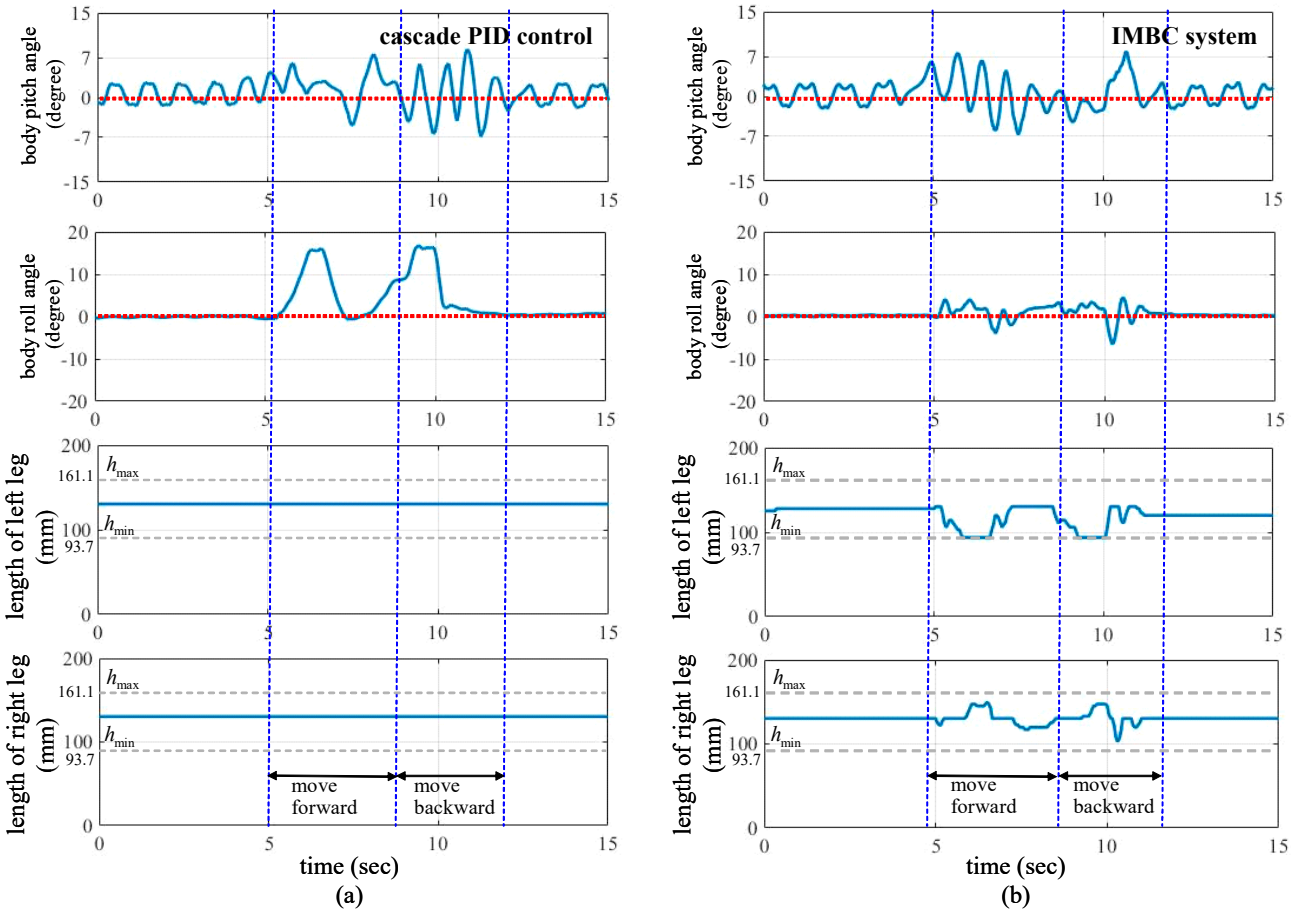

Figure 10. Results of one leg on slope moving. (**a**) Cascade PID control; (**b**) the IMBC system.

5. Conclusions

Due to the non-linear and under-actuated nature of the wheeled bipedal robot (WBR) system, this study presented an intelligent motion and balance control (IMBC) method based on the fuzzy logic approach. It should be emphasized that the IMBC system allows for stability and drive control and does not require the same system dynamics and system parameters of a WBR. Besides the simplicity of design, many other advantages are offered by the proposed control method (such as robustness against external disturbance and parameters variation). Four experimental scenarios, namely moving and rotating, height-changing, posture-keeping, and one leg on slope movement, were tested to explore the stability performance of the IMBC system for the WBR. The experimental results showed that the proposed IMBC system is capable of providing appropriate control outputs to maintain the body balance of the robot, as well as the motion and steering control of the robot, even under variable environmental terrain and with changing robot height. Meanwhile, the video showing the IMBC system for WBR can be found at https://www.youtube.com/watch?v=AR6yP99sSjs (accessed on 20 November 2022). However, the IMBC system depends to a large extent on the expert's knowledge or on trial and error. It was not easy to guarantee the stability and robustness of the closed-loop control systems.

Future works in this study may focus on: (1) Giving a more systematic way to apply external forces to provide a more specific description of performance comparisons. (2) Utilizing Type-2 fuzzy systems [44] to handle the rule uncertainties when it is hard to exactly determine the grade of membership functions. (3) Auto-tuning a fuzzy controller [45,46], whose fuzzy rules can be tuned online without requiring time-consuming adjustments, is developed to ensure the stability of the closed-loop system. (4) Detecting dynamic obstacle

and road features using LiDAR and CCD images to develop an autonomous navigation framework [47,48] that interacts with humans.

Author Contributions: Conceptualization, C.-F.H. and B.-R.C.; Methodology, C.-F.H.; Software, B.-R.C. and Z.-L.L.; Validation, B.-R.C. and Z.-L.L.; Formal Analysis, B.-R.C. and Z.-L.L.; Investigation, C.-F.H. and Z.-L.L.; Resources, C.-F.H.; Data Curation, B.-R.C.; Writing—Original Draft Preparation, C.-F.H. and B.-R.C.; Writing—Review and Editing, C.-F.H. and B.-R.C.; Visualization, B.-R.C.; Supervision, C.-F.H.; Project Administration, C.-F.H.; Funding Acquisition, C.-F.H. All authors have read and agreed to the published version of the manuscript.

Funding: The study was funded by the Ministry of Science and Technology of Republic of China under Grant MOST 108-2221-E-032-039-MY2.

Data Availability Statement: Not applicable.

Acknowledgments: We thank the anonymous reviewers for providing critical comments and suggestions that improved the manuscript.

Conflicts of Interest: The authors declare no conflict of interest.

Appendix A

θ	body pitch angle
ψ	body yaw angle
ϕ	body roll angle
θ_w	robot position
θ_R	rotary angle of the right wheel motor
θ_L	rotary angle of the left wheel motor
R	wheel radius
W	half of body width
L	distance of CoG from the wheel axle
m	wheel weight
M	body weights
J_W	wheel inertia moment
J_θ	body pitch inertia moment
g	gravity acceleration
R_m	wheel motor resistance
K_t	wheel motor torque constant
K_b	wheel motor back electromotive force coefficient
J_m	wheel motor inertia moment
L_1	length between the pin joint and the knee joint
L_2	length between the pin joint and the leg joint
L_3	length between the knee joint and the inner joint
L_4	length between the inner joint and the wheel motor
h	robot height
h_L	height of the left side of the WBR
h_R	height of the right side of the WBR
θ_{kL}	rotary angle of the left leg motor
θ_{kR}	rotary angle of the right leg motor

References

1. McGinn, C.; Cullinan, M.F.; Otubela, M.; Kelly, K. Design of a terrain adaptive wheeled robot for human-orientated environments. *Auton. Robot.* **2019**, *43*, 63–78. [CrossRef]
2. Xu, S.S.D.; Huang, H.C.; Kung, Y.C.; Chu, Y.Y. A networked multirobot CPS with artificial immune fuzzy optimization for distributed formation control of embedded mobile robots. *IEEE Trans. Ind. Inform.* **2020**, *16*, 414–422. [CrossRef]
3. Pang, L.; Cao, Z.; Yu, J.; Guan, P.; Chen, X.; Zhang, W. A robust visual person-following approach for mobile robots in disturbing environments. *IEEE Syst. J.* **2020**, *14*, 2965–2968. [CrossRef]
4. Tazaki, Y.; Murooka, M. A survey of motion planning techniques for humanoid robots. *Adv. Robot.* **2020**, *34*, 1370–1379. [CrossRef]
5. Li, T.H.S.; Kuo, P.H.; Cheng, C.H.; Hung, C.C.; Luan, P.C.; Chang, C.H. Sequential sensor fusion-based real-time LSTM gait pattern controller for biped robot. *IEEE Sens. J.* **2021**, *21*, 2241–2255. [CrossRef]
6. Lee, J.; Bakolas, E.; Sentis, L. An efficient and direct method for trajectory optimization of robots constrained by contact kinematics and forces. *Auton. Robot.* **2021**, *45*, 135–153. [CrossRef]
7. Viragh, Y.; Bjelonic, M.; Bellicoso, C.D.; Jenelten, F.; Hutter, M. Trajectory optimization for wheeled-legged quadrupedal robots using linearized zmp constraints. *IEEE Robot. Autom. Lett.* **2019**, *4*, 1633–1640. [CrossRef]
8. Medeiros, V.S.; Jelavic, E.; Bjelonic, M.; Siegwart, R.; Meggiolaro, M.A.; Hutter, M. Trajectory optimization for wheeled-legged quadrupedal robots driving in challenging terrain. *IEEE Robot. Autom. Lett.* **2020**, *5*, 4172–4179. [CrossRef]
9. Sun, J.; You, Y.; Zhao, X.; Adiwahono, A.H.; Chew, C.M. Towards more possibilities: Motion planning and control for hybrid locomotion of wheeled-legged robots. *IEEE Robot. Autom. Lett.* **2020**, *5*, 3723–3730. [CrossRef]
10. Li, J.; Wang, J.; Peng, H.; Hu, Y.; Su, H. Fuzzy-torque approximation-enhanced sliding mode control for lateral stability of mobile robot. *IEEE Trans. Syst. Man Cybern. Syst.* **2022**, *52*, 2491–2500. [CrossRef]
11. He, J.; Sun, Y.; Yang, L.; Sun, J.; Xing, Y.; Gao, F. Design and control of TAWL-a wheel-legged rover with terrain-adaptive wheel speed allocation capability. *IEEE/ASME Trans. Mechatron.* **2022**, *27*, 2212–2223. [CrossRef]
12. Wang, S.; Chen, Z.; Li, J.; Wang, J.; Li, J.; Zhao, J. Flexible motion framework of the six wheel-legged robot: Experimental results. *IEEE/ASME Trans. Mechatron.* **2022**, *27*, 2246–2257. [CrossRef]
13. Chiu, C.H.; Peng, Y.F.; Sun, C.H. Intelligent decoupled controller for mobile inverted pendulum real-time implementation. *J. Intell. Fuzzy Syst.* **2017**, *32*, 3809–3820. [CrossRef]
14. Huang, J.; Ri, M.; Wu, D.; Ri, S. Interval type-2 fuzzy logic modeling and control of a mobile two-wheeled inverted pendulum. *IEEE Trans. Fuzzy Syst.* **2018**, *26*, 2030–2038. [CrossRef]
15. Su, Y.; Wang, T.; Zhang, K.; Yao, C.; Wang, Z. Adaptive nonlinear control algorithm for a self-balancing robot. *IEEE Access* **2020**, *8*, 3751–3760. [CrossRef]
16. Iwendi, C.; Alqarni, M.A.; Anajemba, J.H.; Alfakeeh, A.S.; Zhang, Z.; Bashir, A.K. Robust navigational control of a two-wheeled self-balancing robot in a sensed environment. *IEEE Access* **2019**, *7*, 82337–82348. [CrossRef]
17. Sekiguchi, S.; Yorozu, A.; Kuno, K.; Okada, M.; Watanabe, Y.; Takahashi, M. Human-friendly control system design for two-wheeled service robot with optimal control approach. *Robot. Auton. Syst.* **2020**, *131*, 103562. [CrossRef]
18. Li, C.H.G.; Zhou, L.P.; Chao, Y.H. Self-balancing two-wheeled robot featuring intelligent end-to-end deep visual-steering. *IEEE/ASME Trans. Mechatron.* **2021**, *26*, 2263–2273. [CrossRef]
19. Li, X.; Zhou, H.; Feng, H.; Zhang, S.; Fu, Y. Design and experiments of a novel hydraulic wheel-legged robot (WLR). In Proceedings of the IEEE/RSJ International Conference on Intelligent Robots and Systems, Madrid, Spain, 1–5 October 2018; pp. 3292–3297.
20. Li, X.; Zhou, H.; Zhang, S.; Feng, H.; Fu, Y. WLR-II, a hose-less hydraulic wheel-legged robot. In Proceedings of the IEEE/RSJ International Conference on Intelligent Robots and Systems, Macau, China, 3–8 November 2019; pp. 4339–4346.
21. Klemm, V.; Morra, A.; Salzmann, C.; Tschopp, F.; Bodie, K.; Gulich, L.; Küng, N.; Mannhart, D.; Pfister, C.; Vierneisel, M.; et al. Ascento: A two-wheeled jumping robot. In Proceedings of the International Conference on Robotics and Automation, Montreal, QC, Canada, 20–24 May 2019; pp. 7515–7521.
22. Zhang, C.; Liu, T.; Song, S.; Meng, M.Q.H. System design and balance control of a bipedal leg-wheeled robot. In Proceedings of the IEEE International Conference on Robotics and Biomimetics, Dali, China, 6–8 December 2019; pp. 1869–1874.
23. Zhao, L.; Yu, Z.; Chen, X.; Huang, G.; Wang, W.; Han, L.; Qiu, X.; Zhang, X.; Huang, Q. System design and balance control of a novel electrically-driven wheel-legged humanoid robot. In Proceedings of the IEEE International Conference on Unmanned Systems, Beijing, China, 15–17 October 2021; pp. 742–747.
24. Raza, F.; Hayashibe, M. Towards robust wheel-legged biped robot system: Combining feedforward and feedback control. In Proceedings of the IEEE/SICE International Symposium on System Integrations, Iwaki, Fukushima, Japan, 11–14 January 2021; pp. 606–612.
25. Dong, J.; Liu, R.; Lu, B.; Guo, X.; Liu, H. LQR-based balance control of two-wheeled legged robot. In Proceedings of the 41st Chinese Control Conference, Hefei, China, 25–27 July 2022; pp. 450–455.
26. Zhou, H.; Yu, H.; Li, X.; Feng, H.; Zhang, S.; Fu, Y. Configuration transformation of the wheel-legged robot using inverse dynamics control. In Proceedings of the IEEE International Conference on Robotics and Automation, Xi'an, China, 30 May–5 June 2021; pp. 3091–3096.
27. Hao, Y.; Lu, B.; Cao, H.; Dong, J.; Liu, R. Run-and-jump planning and control of a compact two-wheeled legged robot. In Proceedings of the 7th Asia-Pacific Conference on Intelligent Robot Systems, Tianjin, China, 1–3 July 2022; pp. 1–6.

28. Xin, Y.; Chai, H.; Li, Y.; Rong, X.; Li, B.; Li, Y. Speed and acceleration control for a two wheel-leg robot based on distributed dynamic model and whole-body control. *IEEE Access* **2019**, *7*, 180630–180639. [CrossRef]
29. Klemm, V.; Morra, A.; Gulich, L.; Mannhart, D.; Rohr, D.; Kamel, M.; Viragh, Y.; Siegwart, R. LQR-assisted whole-body control of a wheeled bipedal robot with kinematic loops. *IEEE Robot. Autom. Lett.* **2020**, *5*, 3745–3752. [CrossRef]
30. Xin, Y.; Vijayakumar, S. Online dynamic motion planning and control for wheeled biped robots. In Proceedings of the IEEE/RSJ International Conference on Intelligent Robots and Systems, Las Vegas, NV, USA, 24 October–24 January 2020; pp. 3892–3899.
31. Wang, Y.; Xin, Y.; Rong, X.; Li, Y. Whole-body motion planning and control for underactuated wheeled-bipdal robots. In Proceedings of the IEEE International Conference on Robotics and Biomimetics, Sanya, China, 27–31 December 2021; pp. 1071–1076.
32. Chen, H.; Wang, B.; Hong, Z.; Shen, C.; Wensing, P.M.; Zhang, W. Underactuated motion planning and control for jumping with wheeled-bipedal robots. *IEEE Robot. Autom. Lett.* **2021**, *6*, 747–754. [CrossRef]
33. Zhu, W.; Raza, F.; Hayashibe, M. Reinforcement learning based hierarchical control for path tracking of a wheeled bipedal robot with sim-to-real framework. In Proceedings of the IEEE/SICE International Symposium on System Integration, Narvik, Norway, 9–12 January 2022; pp. 40–46.
34. Cui, L.; Wang, S.; Zhang, J.; Zhang, D.; Lai, J.; Zheng, Y.; Zhang, Z.; Jiang, Z.P. Learning-based balance control of wheel-legged robots. *IEEE Robot. Autom. Lett.* **2021**, *6*, 7667–7674. [CrossRef]
35. Chang, H.T.; Tai, F.C.; Tsai, C.C. Adaptive fuzzy-basis-function-network trajectory tracking for a terrain-adaptive self-balancing two-wheeled mobile robot. In Proceedings of the International Conference on Fuzzy Theory and Its Applications, Taitung, Taiwan, 5–8 October 2021; pp. 42–47.
36. Wu, C.F.; Chen, B.S.; Zhang, W. Multiobjective investment policy for a nonlinear stochastic financial system: A fuzzy approach. *IEEE Trans. Fuzzy Syst.* **2017**, *25*, 460–474. [CrossRef]
37. Wu, L.F.; Li, T.H.S. Fuzzy dynamic gait pattern generation for real-time push recovery control of a teen-sized humanoid robot. *IEEE Access* **2020**, *8*, 36441–36453. [CrossRef]
38. Zhong, Z.; Zhu, Y.; Lin, C.M.; Huang, T. A fuzzy control framework for interconnected nonlinear power networks under TDS attack: Estimation and compensation. *J. Frankl. Inst.* **2021**, *358*, 74–88. [CrossRef]
39. Benzaouia, S.; K.M'Sirdi, N.; Rabhi, A.; Zouggar, S. Signed-distance fuzzy-logic sliding-mode control strategy for floating interleaved boost converter. In Proceedings of the 9th International Conference on Systems and Control, Caen, France, 24–26 November 2021; pp. 417–422.
40. Choi, B.J.; Kwak, S.W.; Kim, B.K. Design of a single-input fuzzy logic controller and its properties. *Fuzzy Sets Syst.* **1999**, *106*, 299–308. [CrossRef]
41. Londhe, P.S.; Santhakumar, M.; Patre, B.M.; Waghmare, L.M. Task space control of an autonomous underwater vehicle manipulator system by robust single-input fuzzy logic control scheme. *IEEE J. Ocean. Eng.* **2017**, *42*, 13–28. [CrossRef]
42. Li, I.H. Design for a fluidic muscle active suspension using parallel-type interval type-2 fuzzy sliding control to improve ride comfort. *Int. J. Fuzzy Syst.* **2022**, *24*, 1719–1734. [CrossRef]
43. Hsu, C.F.; Kao, W.F. Double-loop fuzzy motion control with CoG supervisor for two-wheeled self-balancing assistant robots. *Int. J. Dyn. Control* **2020**, *8*, 851–866. [CrossRef]
44. Nafia, N.; Kari, A.E.; Ayad, H.; Mjahed, M. Robust interval type-2 fuzzy sliding mode control design for robot manipulators. *Robotics* **2018**, *7*, 40. [CrossRef]
45. Hsu, C.F.; Kao, W.F. Perturbation wavelet-neural sliding-mode position control for a voice coil motor driver. *Neural Comput. Appl.* **2019**, *31*, 5975–5988. [CrossRef]
46. Lin, C.M.; Nguyen, H.B.; Huynh, T.T. A new self-organizing double function-link brain emotional learning controller for MIMO nonlinear systems using sliding surface. *IEEE Access* **2021**, *9*, 73826–73842. [CrossRef]
47. Ye, W.; Li, Z.; Yang, C.; Sun, J.; Su, C.Y.; Lu, R. Vision-based human tracking control of a wheeled inverted pendulum robot. *IEEE Trans. Cybern.* **2016**, *46*, 2423–2434. [CrossRef] [PubMed]
48. Li, J.; Qin, H.; Wang, J.; Li, J. OpenStreetMap-based autonomous navigation for the four wheel-legged robot via 3D-lidar and CCD camera. *IEEE Trans. Ind. Electron.* **2022**, *69*, 2708–2717. [CrossRef]